Analog differential-phase detection in optical coherence reflectometer

Huan-Jang Huang[1], Tsung-Yu Hsieh[2], Li-Dek Chou[1], Wen-Chuan Kuo[3], and Chien Chou[1,2,*]

[1] *Department of Biomedical Imaging and Radiological Sciences, National Yang-Ming University, Taipei 112, Taiwan*
[2] *Institute of Biophotonics, National Yang-Ming University, Taipei 112, Taiwan*
[3] *Institute of Electro-optical Science and Technology, National Taiwan Normal University, Taipei 116, Taiwan*
[*] *Corresponding author: cchou@ym.edu.tw*

Abstract: A novel differential-phase optical coherence reflectometer (DP-OCR) was proposed using a low-coherence source, integrating it with an analog differential-phase decoding method. In the experiment, the DP-OCR performed a localized surface profile measurement of an optical grating (1200 lp/mm) and demonstrated its ability to measure the translation speed of a tilted mirror. Experimentally, the resolution of the axial displacement of proposed DP-OCR at 185 pm was demonstrated.

©2008 Optical Society of America

OCIS codes: (110.3175) Densitometers, reflectometers; (110.4500) Optical coherence tomography; (120.3180) Interferometry; (120.5050) Phase measurement; (120.6660) Surface measurements, roughness.

References and links

1. T. Kubota, M. Nara, and T. Yoshino, "Interferometer for measuring displacement and distance," Opt. Lett. **12**, 310-312 (1987).
2. G. Lai and T. Yatagai, "Generalized phase-shifting interferometry," J. Opt. Soc. Am. A **8**, 822-827 (1991).
3. C. Chou, J.C. Shyu, Y. C. Huang, and C. K. Yuan, "Common-path optical heterodyne profilometer: a configuration," Appl. Opt. **37**, 4137-4142 (1998).
4. C. K. Hitzenberger and A. F. Fercher, "Differential phase contrast in optical coherence tomography," Opt. Lett. **24**, 622-624 (1999).
5. S. Yazdanfar and J. A. Izatt, "Self-referenced Doppler optical coherence tomography," Opt. Lett. **27**, 2085-2087 (2002).
6. C. Chou, C. W. Lyu, and L. C. Peng, "Polarized differential-phase laser scanning microscope," Appl. Opt. **40**, 96-99 (2001).
7. J. W. Goodman, *Introduction to Fourier Optics, 3rd ed.*, (Roberts and Company, Englewood, 2005).
8. S. Haykin, *Communication Systems, 4th Ed.*, (Wiley, New York, 2001).
9. D. P. Dave and T. E. Milner, "Optical low-coherence reflectometer for differential phase measurement," Opt. Lett. **25**, 227-229 (2000).
10. D. Reolon, M. Jacquot, I. Verrier, G. Brun, and C. Veillas, "Broadband supercontinuum interferometer for high-resolution profilometry," Opt. Express **14**, 128-137 (2006).
11. T. Dresel, G. Hausler, and H. Venzke, "Three-dimensional sensing of rough surfaces by coherence radar," Appl. Opt. **31**, 919-925 (1992).
12. L. Deck and P. de Groot, "High-speed noncontact profiler based on scanning white-light interferometry," Appl. Opt. **33**, 7334-7338 (1994).
13. D. Huang, E. A. Swanson, C. P. Lin, J. S. Shuman, W. G. Stinson, W. Chang, M. R. Hee, T. Flottee, K. Gregory, C. A. Puliafito, and J. G. Fujimoto, "Optical coherence tomography," Science **254**, 1178-1181 (1991).
14. J. F. de Boer, T. E. Milner, M. C. J. van Gemert, and J. S. Nelson, "Two-dimensional birefringence imaging in biological tissue by polarization-sensitive optical coherence tomography," Opt. Lett. **22**, 934-936 (1997).
15. U. Morgner, W. Drexler, F. X. Kartner, X. D. Li, C. Pitris, E. P. Ippen, and J. G. Fujimoto, "Spectroscopic optical coherence tomography," Opt. Lett. **25**, 111-113 (2000).
16. T. H. Ko, D. C. Adler, and J. G. Fujimoto, "Ultrahigh resolution optical coherence tomography imaging with a broadband superluminescent diode light source," Opt. Express **12**, 2112-2119 (2004).
17. C. G. Rylander, D. P. Dave, T. Akkin, T. E. Milner, K. R. Diller, and A. J. Welch, "Quantitative phase-contrast imaging of cells with phase-sensitive optical coherence microscopy," Opt. Lett. **29**, 1509-1511 (2004).
18. M. Sticker, M. Pircher, E. Gotzinger, H. Sattmann, A. F. Fercher, and C. K. Hitzenberger, "En Face imaging of single cell layers by differential phase-contrast optical coherence microscopy," Opt. Lett. **27**, 1126-1128 (2002).

#96406 - $15.00 USD Received 20 May 2008; revised 9 Jul 2008; accepted 22 Jul 2008; published 8 Aug 2008

19. M. A. Choma, A. K. Ellerbee, and C. Yang, “Spectral-domain phase microscopy,” Opt. Lett. **30**, 1162-1164 (2005).
20. C. Joo, T. Akkin, B. Cense, B. H. Park, and J. F. de Boer, “Spectral-domain optical coherence phase microscopy for quantitative phase-contrast imaging,” Opt. Lett. **30**, 2131-2133 (2005).
21. C. Joo, K. H. Kim, and J. F. de Boer, “Spectral-domain optical coherence phase and multiphoton microscopy,” Opt. Lett. **32**, 623-625 (2007).
22. D. C. Adler, R. Huber, and J. G. Fujimoto, “Phase-sensitive optical coherence tomography at up to 370,000 lines per second using buffered Fourier domain mode-locked lasers,” Opt. Lett. **32**, 626-628 (2007).
23. C. Hitzenberger, E. Goetzinger, M. Sticker, M. Pircher, and A. Fercher, "Measurement and imaging of birefringence and optic axis orientation by phase resolved polarization sensitive optical coherence tomography," Opt. Express **9**, 780-790 (2001).
24. C. J. Pedersen, D. Huang, M. A.Shure, A. M.Rollins, “Measurement of absolute flow velocity vector using dual-angle, delay-encoded Doppler optical coherence tomography,” Opt. Lett. **32**, 506-508, (2007).
25. R. E. Ziemer and W. H. Tranter, *Principle of communications: Systems, modulation, and noise*, (Houghton Mifflin Co., Boston, MA, 1976).
26. C. Chou, H. K. Teng, C. C. Tsai, and L. P. Yu, “Balanced detector interferometric ellipsometer,” J. Opt. Soc. Am. A, **23**, 2871-2879 (2006).
27. Z. Chen, T. E. Milner, S. Srinivas, X. Wang, A. Malekafzali, M. J. C. van Gemert, and J. S. Nelson, “Noninvasive imaging of in vivo blood flow velocity using optical Doppler tomography,” Opt. Lett. **22**, 1119-1121 (1997).
28. H. Lim, J. F. de Boer, B. H. Park, E. C. Lee, R. Yelin, and S. H. Yun, “Optical frequency domain imaging with a rapidly swept laser in the 815-870 nm range,” Opt. Express **14**, 5937-5944 (2006).
29. C. Tsai, H. Wei, S. Huang, C. Lin, C. Yu, and C. Chou, "High speed interferometric ellipsometer," Opt. Express **16**, 7778-7788 (2008).
30. D. P. Davé and T. E. Milner, "Optical low-coherence reflectometer for differential phase measurement," Opt. Lett. **25**, 227-229 (2000).
31. C. Yang, A. Wax, I. Georgakoudi, E. B. Hanlon, K. Badizadegan, R. R. Dasari, and M. S. Feld, "Interferometric phase-dispersion microscopy," Opt. Lett. **25**, 1526-1528 (2000).

1. Introduction

Interferometer-based surface profile measurements have been developed for many years [1, 2]. Most interferometers use monochromatic light sources and measure displacement by obtaining the phase information through decoding phase difference utilizing various analog methods such as a lock-in amplifier [3]. However, this method results in a slower response of the phase decoding. Moreover, decoding phase differences via numerical method through Hilbert transformation [4] or autocorrelation algorithm [5] was proposed. The analog method is therefore preferred when attempting to obtain a precise measurement of localized surface profiles because it possesses the advantage of higher sensitivity from its high time-bandwidth product [3,6-8]. Recently, low coherence surface profilometers have been developed based on low coherence interferometers [9-11]. This includes the scanning white-light interferometer (SWLI) [12] and the optical coherence tomography (OCT) [13-15], both of which are used for various applications. These interferometers have short temporal coherence lengths represented by $2(\ln 2)\lambda_0^2/(\pi\Delta\lambda)$ for localized surface measurements, where λ_0 is the central wavelength and $\Delta\lambda$ is the spectral bandwidth. Thus, they can acquire tomographic images based on a low coherence length of the laser source. For a superluminescent diode (SLD) with the spectral bandwidth equal to 155 nm, almost 2 μm axial resolution of OCT was obtained [16]. However, this system cannot measure a structure smaller than 2 μm in thickness variation through intensity response. Hence, various phase-sensitive detection methods, such as differential phase-contrast optical coherence tomography (DPC-OCT) [4] and microscopy (DPC-OCM) [17,18], spectral-domain phase microscopy (SDPM) [19], spectral-domain optical coherence phase microscopy(SD-OCPM) [20,21], and phase-sensitive OCT using Fourier domain mode-locked laser (FDML-PSOCT) [22], are proposed. All of these detection methods are in time or frequency domain. Among them, the SD-OCPM and FDML-PSOCT, which utilize a wider spectral range of low coherence sources, have the capability to acquire axial displacement and localize the surface profile with higher sensitivity compared to other methods using a narrower spectral range SLD in a conventional OCT. The stability and sensitivity of SD-OCPM and FDML-PSOCT on axial displacement are therefore enhanced to the sub-nanometer level [21, 22]. Both methods, however, decode the phase variation

#96406 - $15.00 USD Received 20 May 2008; revised 9 Jul 2008; accepted 22 Jul 2008; published 8 Aug 2008
(C) 2008 OSA

numerically. Thus, the phase decoding speed is determined by the data sampling rate. Additionally, a low numerical aperture (NA) objective is adopted in their systems, thereby resulting in less lateral resolution as well. In this experiment, the proposed differential-phase optical coherence reflectometer (DP-OCR) is set up, wherein an SLD is employed as the light source. An analog differential-phase decoding method [6] is integrated in the DP-OCR for localized surface profile measurement. Similar to SD-OCPM and FDML-PSOCT, the DP-OCR stability on axial displacement was measured and shown with sub-nanometer sensitivity in this experiment. The surface profile of an optical grating at 1200 lp/mm was also scanned. In addition, the translation speed of a tilted mirror was demonstrated as well by measuring the Doppler frequency shift successfully. The comparison between the DP-OCR and the atomic force microscope (AFM) on the surface profile measurement of an optical grating was then discussed. Finally, a novel DP-OCR simultaneously presenting high resolution on axial displacement and high lateral resolution based on a high NA objective and SLD on a localized surface profile measurement was experimentally verified.

2. Principle of Differential-phase optical coherence reflectometer

The experimental setup of DP-OCR is shown in Fig. 1. A SLD is employed as a low coherence light source emitting an elliptically polarized beam. The beam goes through three components composed of a half wave plate (HWP), a polarization beam splitter (PBS1), and a quarter wave plate (QWP) to establish an optical isolator resulting in a circularly polarized output beam. The beam can then be described by Jones vector as

$$E = E_0 \begin{pmatrix} 1 \\ \pm i \end{pmatrix}, \tag{1}$$

where $E_0 = A_0(k)\exp[i(\omega t)]$ and $A_0(k)$ denotes the electric field amplitude which is a function of the wave number $k = 2\pi/\lambda$.

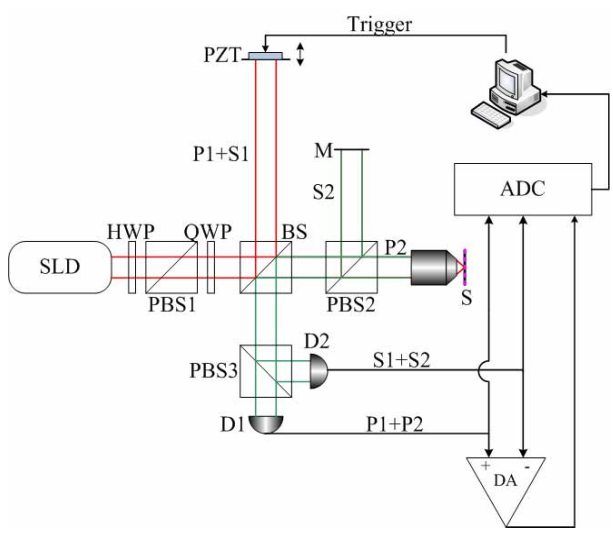

Fig. 1. Schematic diagram of DP-OCR: HWP, half wave plate; QWP, quarter wave plate; BS, beam splitter; PBS1, PBS2, PBS3, polarization beam splitters; D1, D2, photo detectors; DA, differential amplifier; ADC, analog-to-digital converter; S, sample; M, mirror; PZT, piezoelectric-supported mirror.

#96406 - $15.00 USD Received 20 May 2008; revised 9 Jul 2008; accepted 22 Jul 2008; published 8 Aug 2008
(C) 2008 OSA

In Eq. (1), the electric field can be decomposed into one horizontal ($E_{\mathrm{P}} = E_0[1,0]^T$) and one vertical ($E_{\mathrm{S}} = E_0[0,\pm i]^T$) polarization component, where the superscript T denotes the transpose. If the laser beam is right-hand circularly polarized, after being split by a 50:50 beam splitter (BS) into two equal-amplitude laser beams, then the reference beam and signal beam are

$$E_1 = \frac{1}{\sqrt{2}} E_0 \begin{pmatrix} 1 \\ i \end{pmatrix}, \tag{2}$$

$$E_2 = \frac{1}{\sqrt{2}} E_0 \begin{pmatrix} 1 \\ i \end{pmatrix}, \tag{3}$$

respectively. In the reference arm, PZT is modulated at a certain frequency to generate Doppler frequency shift, and the reference beam reflected by PZT is decomposed into P1 wave and S1 wave by PBS3. The signal beam is split by PBS2 into two orthogonal linearly polarized waves, denoted as the P2 wave and the S2 wave, which are expressed by

$$E_{\mathrm{P2}} = \sqrt{\frac{R_{\mathrm{S}}}{2}} E_0 \begin{pmatrix} 1 \\ 0 \end{pmatrix} \exp(-i2kl_{\mathrm{P2}}), \tag{4}$$

$$E_{\mathrm{S2}} = \sqrt{\frac{R_{\mathrm{M}}}{2}} E_0 \begin{pmatrix} 0 \\ i \end{pmatrix} \exp(-i2kl_{\mathrm{S2}}), \tag{5}$$

where R_{S} and R_{M} are the reflectivity of S and M, respectively. The l_{P2} and l_{S2} are the optical path lengths of P2 and S2 waves in the interferometer, respectively. The P2 wave is then focused by an objective (60X, NA=0.85, Olympus) onto the surface of the specimen (S) as the signal beam, and the S2 wave is reflected by M as the reference beam. Thus, two P waves (P1+P2) and two S waves (S1+S2) are recombined and then separated by PBS3, resulting in P- and S-polarized optical heterodyned signals at photo detectors D1 and D2, respectively. The electric fields of P1, P2, S1, and S2 are

$$E_{\mathrm{P1}} = \frac{\sqrt{R_1}}{2} E_0 \begin{pmatrix} 1 \\ 0 \end{pmatrix} \exp(-i2kl_{\mathrm{P1}}), \tag{6}$$

$$E_{\mathrm{P2}} = \frac{\sqrt{R_{\mathrm{S}}}}{2} E_0 \begin{pmatrix} 1 \\ 0 \end{pmatrix} \exp(-i2kl_{\mathrm{P2}}), \tag{7}$$

$$E_{\mathrm{S1}} = \frac{\sqrt{R_1}}{2} E_0 \begin{pmatrix} 0 \\ i \end{pmatrix} \exp(-i2kl_{\mathrm{S1}}), \tag{8}$$

$$E_{\mathrm{S2}} = \frac{\sqrt{R_{\mathrm{M}}}}{2} E_0 \begin{pmatrix} 0 \\ i \end{pmatrix} \exp(-i2kl_{\mathrm{S2}}), \tag{9}$$

where R_1 is the reflectivity of the mirror mounted on PZT, and l_{P1} and l_{S1} are the optical path lengths of P1 and S1 waves in the interferometer, respectively. Thus,

$$E_{\mathrm{P}} = \frac{1}{2} E_0 \left[\sqrt{R_1} \exp(-i2kl_{\mathrm{P1}}) + \sqrt{R_{\mathrm{S}}} \exp(-i2kl_{\mathrm{P2}}) \right], \tag{10}$$

#96406 - $15.00 USD Received 20 May 2008; revised 9 Jul 2008; accepted 22 Jul 2008; published 8 Aug 2008
(C) 2008 OSA

$$E_{\mathrm{S}} = \frac{i}{2} E_0 \left[\sqrt{R_1} \exp(-i2kl_{\mathrm{S1}}) + \sqrt{R_{\mathrm{M}}} \exp(-i2kl_{\mathrm{S2}}) \right], \tag{11}$$

$$\begin{aligned} i_P &= \gamma \left\langle E_P^2 \right\rangle \\ &= \frac{\gamma A_0^2(k)}{4} \left[R_1 + R_{\mathrm{S}} + 2\sqrt{R_1 R_{\mathrm{S}}} \cos(2k\Delta l_{\mathrm{P}}) \right], \end{aligned} \tag{12}$$

$$\begin{aligned} i_S &= \gamma \left\langle E_S^2 \right\rangle \\ &= \frac{\gamma A_0^2(k)}{4} \left[R_1 + R_{\mathrm{M}} + 2\sqrt{R_1 R_{\mathrm{M}}} \cos(2k\Delta l_{\mathrm{S}}) \right], \end{aligned} \tag{13}$$

where γ is the quantum efficiency of photo detectors, and $\Delta l_{\mathrm{P}} = l_{\mathrm{P1}} - l_{\mathrm{P2}}$, $\Delta l_{\mathrm{S}} = l_{\mathrm{S1}} - l_{\mathrm{S2}}$. Assume that the power spectrum of SLD, $A_0^2(k)$, satisfies the condition

$$A_0^2(k) = P_0 S(k), \tag{14}$$

where P_0 is the power of the laser source and $S(k)$ is the Gaussian spectral density

$$S(k) = \frac{2\sqrt{\ln 2}}{\Delta k \sqrt{\pi}} \exp\left\{ -\left[\frac{(k-k_0)2\sqrt{\ln 2}}{\Delta k} \right]^2 \right\}, \tag{15}$$

k_0 is the wave number on the central wavelength, and Δk is the spectral bandwidth (FWHM) of the source. The interference signal by integrating the whole spectrum is therefore

$$\begin{aligned} I_{\mathrm{P}} &= \int_{-\infty}^{\infty} i_{\mathrm{P}} dk \\ &= \frac{\gamma P_0}{4} \int_{-\infty}^{\infty} S(k) \left[R_1 + R_{\mathrm{S}} + 2\sqrt{R_1 R_{\mathrm{S}}} \cos(2k\Delta l_{\mathrm{P}}) \right] dk \\ &= \frac{\gamma P_0}{4} \exp\left[-\left(\frac{2\Delta l_{\mathrm{P}} \sqrt{\ln 2}}{l_\omega} \right)^2 \right] \left[R_1 + R_{\mathrm{S}} + 2\sqrt{R_1 R_{\mathrm{S}}} \cos(2k_0 \Delta l_{\mathrm{P}}) \right], \end{aligned} \tag{16}$$

$$\begin{aligned} I_{\mathrm{S}} &= \int_{-\infty}^{\infty} i_{\mathrm{S}} dk \\ &= \frac{\gamma P_0}{4} \int_{-\infty}^{\infty} S(k) \left[R_1 + R_{\mathrm{M}} + 2\sqrt{R_1 R_{\mathrm{M}}} \cos(2k\Delta l_{\mathrm{S}}) \right] dk \\ &= \frac{\gamma P_0}{4} \exp\left[-\left(\frac{2\Delta l_{\mathrm{S}} \sqrt{\ln 2}}{l_\omega} \right)^2 \right] \left[R_1 + R_{\mathrm{M}} + 2\sqrt{R_1 R_{\mathrm{M}}} \cos(2k_0 \Delta l_{\mathrm{S}}) \right], \end{aligned} \tag{17}$$

where the coherence length of the light source is

$$l_\omega = \frac{4\ln 2}{\Delta k} = \frac{2(\ln 2)\lambda_0^2}{\pi \Delta \lambda}, \tag{18}$$

and λ_0 is the central wavelength of the low coherence light source. From Eqs. (16) and (17), the Gaussian profile of the interference signals is subsequently obtained. For simplicity, the condition $\Delta l_{\mathrm{P}} \cong \Delta l_{\mathrm{S}} = \Delta l$ is assumed in this setup when the surface profile being measured is

#96406 - $15.00 USD Received 20 May 2008; revised 9 Jul 2008; accepted 22 Jul 2008; published 8 Aug 2008
(C) 2008 OSA

an optical surface. Thus, $\Delta l << l_\omega$ is satisfied. The differential signal by using a differential amplifier (DA) becomes

$$\begin{aligned} I_{diff} &= \left| I_{\mathrm{P}} - I_{\mathrm{S}} \right| \\ &\cong \left| \frac{\gamma P_0}{4} \exp\left[-\left(\frac{2\Delta l \sqrt{\ln 2}}{l_\omega} \right)^2 \right] \left\{ \left(R_{\mathrm{S}} - R_{\mathrm{M}} \right) + 2\sqrt{R_1} \left[\sqrt{R_{\mathrm{S}}} \cos\left(2k_0 \Delta l_{\mathrm{P}}\right) - \sqrt{R_{\mathrm{M}}} \cos\left(2k_0 \Delta l_{\mathrm{S}}\right) \right] \right\} \right|. \end{aligned} \quad (19)$$

By considering only the AC part of the signal,

$$I_{diff} \cong \frac{\gamma P_0 \sqrt{R_1}}{2} \exp\left[-\left(\frac{2\Delta l \sqrt{\ln 2}}{l_\omega} \right)^2 \right] \left| \sqrt{R_{\mathrm{S}}} \cos\left(2k_0 \Delta l_{\mathrm{P}}\right) - \sqrt{R_{\mathrm{M}}} \cos\left(2k_0 \Delta l_{\mathrm{S}}\right) \right|, \quad (20)$$

where $2k_0 \Delta l_{\mathrm{P}} = \omega_D t + \phi_{\mathrm{P}}$ and $2k_0 \Delta l_{\mathrm{S}} = \omega_D t + \phi_{\mathrm{S}}$ are defined, ω_D is the Doppler frequency shift from the modulation of PZT, and ϕ_{P} and ϕ_{S} are the phase terms corresponding to the path length from PBS2 to S and M, respectively. Therefore,

$$\begin{aligned} I_{diff} &\cong \frac{\gamma P_0 \sqrt{R_1}}{2} \exp\left[-\left(\frac{2\Delta l \sqrt{\ln 2}}{l_\omega} \right)^2 \right] \left| \sqrt{R_{\mathrm{S}}} \cos\left(\omega_D t + \phi_{\mathrm{P}}\right) - \sqrt{R_{\mathrm{M}}} \cos\left(\omega_D t + \phi_{\mathrm{S}}\right) \right| \\ &= \frac{\gamma P_0 \sqrt{R_1}}{2} \exp\left[-\left(\frac{2\Delta l \sqrt{\ln 2}}{l_\omega} \right)^2 \right] \left| \sqrt{R_{\mathrm{S}}} \cos\left(\omega_D t + \phi_{\mathrm{P}} - \phi_{\mathrm{S}}\right) - \sqrt{R_{\mathrm{M}}} \cos\left(\omega_D t\right) \right| \\ &= \frac{\gamma P_0 \sqrt{R_1}}{2} \exp\left[-\left(\frac{2\Delta l \sqrt{\ln 2}}{l_\omega} \right)^2 \right] \left| \cos\left(\omega_D t\right) \left[\sqrt{R_{\mathrm{S}}} \cos\left(\Delta\phi\right) - \sqrt{R_{\mathrm{M}}} \right] + \sin\left(\omega_D t\right) \left[-\sqrt{R_{\mathrm{S}}} \sin\left(\Delta\phi\right) \right] \right| \\ &= \frac{\gamma P_0 \sqrt{R_1}}{2} \exp\left[-\left(\frac{2\Delta l \sqrt{\ln 2}}{l_\omega} \right)^2 \right] \sqrt{R_{\mathrm{S}} + R_{\mathrm{M}} - 2\sqrt{R_{\mathrm{S}} R_{\mathrm{M}}} \cos\left(\Delta\phi\right)} \cos\left(\omega_D t - \theta\right), \end{aligned} \quad (21)$$

where $\Delta\phi = \phi_{\mathrm{P}} - \phi_{\mathrm{S}}$ is the differential-phase. During the derivation, a common phase ϕ_S was shifted in both cosine terms in Eq. (21) because the differential output signal from the differential amplifier (DA) in Fig. 1 is independent of the initial reference point of both heterodyne signals [6]. Then

$$\cos\theta = \frac{\sqrt{R_{\mathrm{S}}} \cos\left(\Delta\phi\right) - \sqrt{R_{\mathrm{M}}}}{\sqrt{R_{\mathrm{S}} + R_{\mathrm{M}} - 2\sqrt{R_{\mathrm{S}} R_{\mathrm{M}}} \cos\left(\Delta\phi\right)}}, \quad (22)$$

$$\sin\theta = \frac{-\sqrt{R_{\mathrm{S}}} \sin\left(\Delta\phi\right)}{\sqrt{R_{\mathrm{S}} + R_{\mathrm{M}} - 2\sqrt{R_{\mathrm{S}} R_{\mathrm{M}}} \cos\left(\Delta\phi\right)}}. \quad (23)$$

In the experiment, peak values of Eqs. (16), (17), and (21) are simultaneously measured using an analog–to-digital converter:

$$I_{\mathrm{P}}^M = Max\left\{ \frac{\gamma P_0 \sqrt{R_1 R_{\mathrm{S}}}}{2} \exp\left[-\left(\frac{2\Delta l \sqrt{\ln 2}}{l_\omega} \right)^2 \right] \cos\left(2k_0 \Delta l_{\mathrm{P}}\right) \right\}, \quad (24)$$

$$I_{\mathrm{S}}^M = Max\left\{ \frac{\gamma P_0 \sqrt{R_1 R_{\mathrm{M}}}}{2} \exp\left[-\left(\frac{2\Delta l \sqrt{\ln 2}}{l_\omega} \right)^2 \right] \cos\left(2k_0 \Delta l_{\mathrm{S}}\right) \right\}, \quad (25)$$

#96406 - $15.00 USD Received 20 May 2008; revised 9 Jul 2008; accepted 22 Jul 2008; published 8 Aug 2008
(C) 2008 OSA

$$I_{diff}^{M} = Max\left\{\frac{\gamma P_0\sqrt{R_1}}{2}\exp\left[-\left(\frac{2\Delta l\sqrt{\ln 2}}{l_\omega}\right)^2\right]\sqrt{R_S + R_M - 2\sqrt{R_S R_M}\cos(\Delta\phi)}\cos(\omega t - \theta)\right\}. \quad (26)$$

In Eq. (26), the differential amplifier's output signal is related to the differential-phase $\Delta\phi$, which varies with the optical path difference of P2 and S2 waves. Finally, the surface height Δh of sample S relative to the reference on M can be calculated by

$$\begin{aligned}\Delta h &= \frac{1}{2}\cdot\frac{\lambda_0}{2\pi}\cdot\Delta\phi \\ &= \frac{\lambda_0}{4\pi}\cos^{-1}\left[\frac{\left(I_S^M\right)^2 + \left(I_P^M\right)^2 - \left(I_{diff}^M\right)^2}{2I_S^M I_P^M}\right]\end{aligned} \quad (27)$$

However, there might be a residual phase bias generated by optical components or a fixed optical path difference between the two beams from PBS2 to M and S in Fig. 1. This results in a constant surface height Δh_0 in the measurement. In order to avoid the occurrence of Δh_0, a calibration procedure is necessary before proceeding with the measurement, wherein the specimen S is replaced by a perfect mirror. The Δh_0 is then obtained, such that the result from Eq. (27) is modified to be

$$\Delta h = \frac{\lambda_0}{4\pi}\cos^{-1}\left[\frac{\left(I_S^M\right)^2 + \left(I_P^M\right)^2 - \left(I_{diff}^M\right)^2}{2I_S^M I_P^M}\right] - \Delta h_0 . \quad (28)$$

3. Experimental setup and results

3.1 DP-OCR configuration and system performance evaluation

In this setup, PZT is modulated at 1Hz frequency and 2 μm longitudinal displacement, resulting in a 4 μm/s average velocity that introduces a ω_D = 60.32 rad/s of Doppler frequency shift. The output power of the elliptically polarized SLD (BWC-SLD11, Superlum) is 2 mW and its spectral bandwidth (FWHM) is 25 nm centered at λ_0 = 827 nm. To prevent the back-reflected laser beam incident into the laser cavity and attain better source stability, an optical isolator composed of a half wave plate (HWP), a polarization beam splitter (PBS), and a quarter wave plate (QWP) was set up as shown in Fig. 1. The bandwidth of the differential amplifier (LeCroy DA 1855A) is capable of 100 MHz in full bandwidth. To test the temporal stability of the DP-OCR, a plane mirror was used as a tested sample and the fluctuation of axial displacement is measured for a specified period of time. The result is shown in Fig. 2, with the standard deviation calculated at 370 pm within 100 seconds of the measurement. The resolution of axial displacement of 185 pm was then achieved because the displacement is twice as large as the surface profile being measured in this experiment. However, it becomes 3 nm when the measurement lasts 10 minutes due to a long term drift of the system brought by environmental disturbance in the interferometer. A quasi-sinusoidal drift of the mirror was apparently produced in the measurement as shown in Fig. 2. The sampling rate of data acquisition in this experiment was 200K sample/s (single channel). According to the equation of $\Delta\Phi=(4\pi/\lambda o)\Delta z$, the differential phase sensitivity becomes $\delta(\Delta\Phi)=(4\pi/\lambda o)\delta(\Delta z)$. Thus, $\delta(\Delta\Phi)= 0.16^o$ is calculated of this DP-OCR in measurement. The SNR=$\Delta z/\delta(\Delta z)$=23 dB was obtained as well in the experiment as shown in Fig. 2. To compare the differential phase sensitivity at 1.8^o via Hilbert transformation [23] and 5.16^o by autocorrelation algorithm [5], it is obviously that DP-OCR performs better differential-phase stability

#96406 - $15.00 USD Received 20 May 2008; revised 9 Jul 2008; accepted 22 Jul 2008; published 8 Aug 2008
(C) 2008 OSA

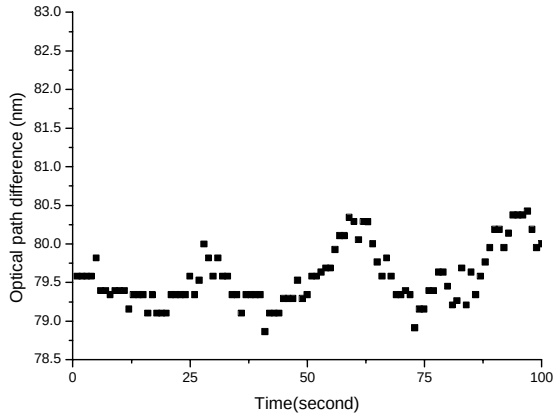

Fig. 2. Stability test of DP-OCR on axial displacement.

In order to verify the DP-OCR principle experimentally, $R_1 \cong R_S \cong R_M = R$ is arranged by using a plane mirror as testing surface. Equations (21), (22), and (23) are then simplified to be

$$I_{diff} = \left| \gamma P_0 R \cdot \exp\left[-\left(\frac{2\Delta l \sqrt{\ln 2}}{l_\omega} \right)^2 \right] \cos\left(\frac{\Delta\phi}{2} \right) \cos\left(\omega_D t - \theta \right) \right|, \tag{29}$$

$$\cos\theta = \cos\left(\frac{\Delta\phi}{2} \right), \tag{30}$$

$$\sin\theta = -\sin\left(\frac{\Delta\phi}{2} \right). \tag{31}$$

To verify Eq. (29) of the output signal from DA, the differential signal variation with respect to the optical path difference produced by displacing the mirror longitudinally at 28 nm on each step was measured using a PZT-controlled precision stage. The experimental results (dots) and theoretical calculation (solid line) in accordance with Eq. (27) are largely consistent with each other as shown in Fig. 3, in which the normalized intensity (V) is defined by

$$V = \frac{\left(I_{diff}^M\right)^2 - \left(I_V^M\right)^2 - \left(I_H^M\right)^2}{2 I_V^M I_H^M} = cos(\Delta\phi) \tag{32}$$

#96406 - $15.00 USD Received 20 May 2008; revised 9 Jul 2008; accepted 22 Jul 2008; published 8 Aug 2008
(C) 2008 OSA

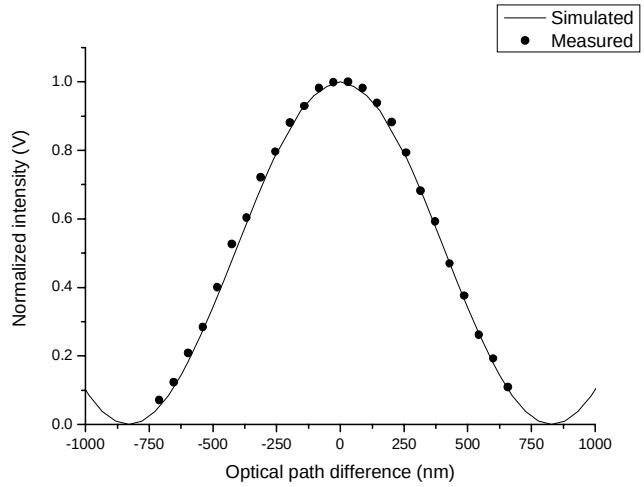

Fig. 3. The measured data (dots) and computer simulation (solid line) of a plane mirror axially displaced at 28 nm in each step by use of DP-OCR. The error bar of the measurement is smaller than the size of dots.

3.2 Surface profile measurement of an optical grating

To demonstrate the performance of the DP-OCR, a one-dimensional surface profile of an optical grating (1200 lp/mm) was measured by laterally scanning it in the experiment. Because of the slow speed of the PZT (1 Hz) in this experiment, it limits the measured speed at one data point per second in this experiment. In Fig. 4, the surface profiles scanned by DP-OCR (dots) and by AFM (solid line) are shown and compared.

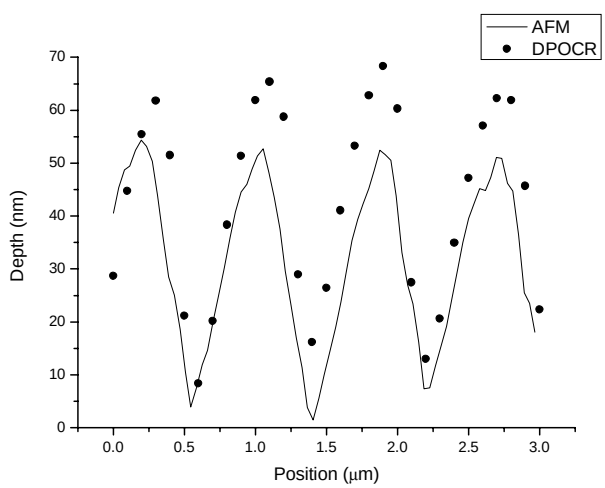

Fig. 4. Surface profile of an optical grating (1200 lp/mm) measured by DP-OCR (dots) and by AFM (solid line). The error bar of the measured data by DP-OCR is less than the size of the dots.

#96406 - $15.00 USD Received 20 May 2008; revised 9 Jul 2008; accepted 22 Jul 2008; published 8 Aug 2008
(C) 2008 OSA

As seen in Fig. 4, the depth of each groove of optical grating is 55 nm in both methods. However, there is a bias on the surface height ($h_0 \cong 8$ nm) between the two measurements. This is due to a residual phase bias attributed by optical components in the DP-OCR. This introduces an optical path difference between P and S polarized heterodyne signals in this measurement. From Fig. 4, it indicates that the principle of DP-OCR is implemental for surface profile measurement.

3.3 Translational velocity measurement of a tilted mirror

To apply DP-OCR in the translational velocity measurement, a tilted mirror was displaced laterally in this experiment to introduce the Doppler frequency shift for velocity measurement in real time. Theoretically, the Doppler shift f_D can be calculated by

$$\begin{aligned} f_D &= \frac{\Delta\phi}{2\pi T} \\ &= \frac{1}{2\pi T}\cos^{-1}\left[\frac{\left(I_{\mathrm{S}}^{M}\right)^2+\left(I_{\mathrm{P}}^{M}\right)^2-\left(I_{diff}^{M}\right)^2}{2I_{\mathrm{S}}^{M}I_{\mathrm{P}}^{M}}\right], \end{aligned} \tag{33}$$

where $\Delta\phi$ and T are the phase difference and the time interval between successive differential-phase measurement, respectively. Thus the translational velocity is calculated [24] by

$$V = \frac{f_D\lambda_0}{2\cos\theta}, \tag{34}$$

where θ is the Doppler angle between the probing beam and the translation direction of the tilted mirror. Figure 5 shows the linear relationship between the translational speed of the electronically driven tilted mirror and the measured Doppler shift. The solid line (red) represents a least squares linear fit to the measured data (blue). In this experiment, the mirror was tilted to set the Doppler angle at 89.75° and the modulation frequency of PZT was 40 Hz. The surface height variation contributing to the differential-phase can be ignored in this phase decoding process in order to ensure the Doppler frequency shift's accuracy because DP-OCR is localized on the tested mirror's surface during the measurement. As a result, the uncertainty in Fig. 5 is minimized if a high quality optical mirror is tested in the experiment. However, it was observed that the higher the speed of the mirror being translated, the larger the uncertainty of the Doppler frequency shifted by the DP-OCR due to the instability of the translation stage, as shown in Fig. 5. The DP-OCR is not only able to provide high sensitivity on speed measurement based on the high time-bandwidth product of differential-phase measurement by way of analog amplitude-sensitive phase decoding method using envelope detection technique [25], it also enables us to reduce excess noise from the laser intensity fluctuation, which implies the possibility of shot-noise-limited detection [6,26]. This experiment is focused on localized surface displacement rather than conventional optical Doppler tomography of the volume medium consideration [27], of which the environmental disturbed phase noise in the tested medium induces the fluctuation on velocity measurement.

#96406 - $15.00 USD Received 20 May 2008; revised 9 Jul 2008; accepted 22 Jul 2008; published 8 Aug 2008
(C) 2008 OSA

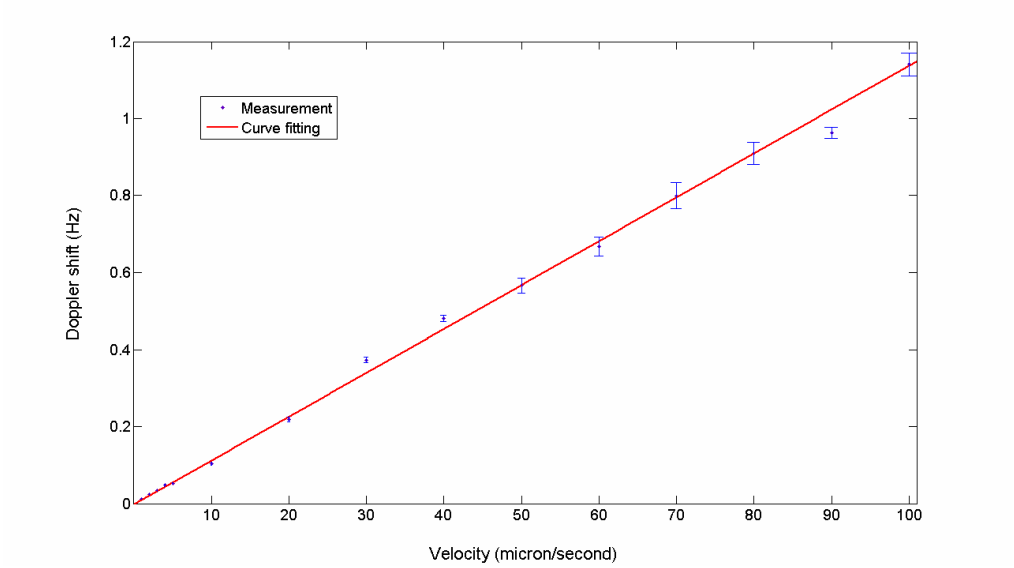

Fig. 5. Linear relationship between the translational speed of tilted mirror and Doppler shift by DP-OCR.

4. Conclusions and discussion

A novel DP-OCR coupled with an analog differential-phase decoding method using a differential amplifier with a low coherence light source and a high NA objective was set up and demonstrated in the experiment. The advantage of DP-OCR is the combination of high NA objective and narrower band width of SLD that result in better surface localization for surface profile measurement under the non-common configuration in Fig. 1. This is equivalent to the case of SD-OCPM and FDML-PSOCT using lower NA objective and broadband laser source to give better depth resolve performance with a common-path configuration and a cover glass. There is a trade-off on Rayleigh region and lateral resolution in DP-OCR and SD-OCPM or FDML-PSOCT. The DP-OCR benefits from the developed analog differential-phase decoding method which can convert phase modulation into amplitude modulation via conventional envelope detection technique. This results in high SNR and phase detection sensitivity via modified balanced detector scheme and synchronized heterodyne detection [6]. Moreover, the developed analog decoding method can achieve large time-bandwidth product, wherein the differential amplifier in the DP-OCR is capable of attaining 100MHz in full bandwidth. This obviously results in higher sensitivity on the surface profile measurement.

Three channels' amplitude modulated heterodyne signals (P wave, S wave, and their difference) are measured simultaneously in DP-OCR. It is not only to decode the difference phase in terms of the demodulated amplitudes of three heterodyne signals simultaneously but also the common phase noise rejection mode as well by use of a differential amplifier. This is critical to the phase decoding sensitivity because high SNR of the detected signal is obtained experimentally. With Hilbert transformation, the correlation between P and S heterodyne signals is degraded numerically. This results in the lower common phase noise rejection ability of phase difference by Hilbert transformation compared with that in DP-OCR. To adopt differential amplifier in DP-OCR mainly the differential-phase is conducted analogically and highly correlated as shown in balanced detector scheme. Besides, the excess noise from the laser intensity fluctuation is reduced too. These are all critical to the improvement on the detection sensitivity of phase decoding in DP-OCR. In the mean time, the sensitivity on envelop detection technique and its fast temporal response are beneficial too. Potentially, DP-OCR is capable of presenting high temporal response when a high speed phase modulator in reference beam is available. This analytical solution of the differential-

#96406 - $15.00 USD Received 20 May 2008; revised 9 Jul 2008; accepted 22 Jul 2008; published 8 Aug 2008
(C) 2008 OSA

phase decoding method in DP-OCR is able to recover the localized surface profile's fine structure at high sensitivity. This is in contrast to the conventional method of using a numerical method with a limited sampling rate to make it difficult to reconstruct surface roughness. As previously discussed, the detection sensitivity and stability on the surface profile are enhanced in DP-OCR because of the analog differential-phase decoding method, which conducts an amplitude sensitive detection in real time. In this experiment, 185 pm on the resolution of axial displacement was achieved by monitoring the stability within 100 seconds. Because the DP-OCR is integrated a conventional SLD of narrow spectral bandwidth (25nm) with a high NA objective, thus, a localized surface profile or translation speed measurement is suitable for DP-OCR. However, DP-OCR is an order of magnitude off from the performance on surface roughness measurement of SD-OCPM [21] and FDML-PSOCT [22] in experiment.

DP-OCR belongs to analog approach rather than in digital domain because the differential amplifier outputs analog signal in real time whereas, the DAQ card samples the output heterodyne signal from differential amplifier in digital domain. This arrangement doesn't lose the feature of the analog approach with high time-bandwidth product on differential-phase decoding in DP-OCR. It is similar to a digital amplifier integrated with an analog preamplifier for high quality signal detection. In other words, three demodulated amplitudes of I_p and I_S and their difference can be obtained simultaneously by using three independent digital voltmeters with envelope detection in DP-OCR as well. The differential-phase is then able to be decoded precisely in real time [29]. Comparison DP-OCR with conventional dual-channel low coherence reflectometers [4,5,30,31], the sensitivity on differential-phase detection is in the range from 0.7^o to 5.16^o. It is in contrast to DP-OCR whereas 0.16^o of the differential-phase stability was obtained in this experiment. Theoretically, the DP-OCR is capable of simultaneously providing high time-bandwidth and space-bandwidth products on a localized surface profile measurement. In comparison with a white light phase-shifting interferometer (PSI) for surface profile measurement, the DP-OCR exhibited the same sensitivity on the resolution of axial displacement [11,12]. However, a better lateral resolution than a PSI-based profilometer is anticipated.

Fundamentally, the DP-OCR is able to be extended into differential-phase polarization sensitive optical coherence tomography (DP-PSOCT) for birefringent phase measurement. DP-OCR can also utilize a swept source in the Fourier domain [27] to become SS-DP-PSOCT, which can further enhance the speed on tomographic phase retardation imaging for biomedical applications.

Acknowledgment

This research was partially supported by National Science Council of Taiwan through Grant # NSC95-2221-E-010-015-MY3. The support by "Aim for top university plan" is also appreciated.